

## Chemical Transport of Rare-Earth Compounds with Complex Anions

Marcus Schmidt, Raul Cardoso-Gil, Sylvia Gerlach, Ulf Müller, and Ulrich Burkhardt

The starting point of this investigation is based on the chemical transport of rare-earth vanadates (V) [1, 2] as well as works by Schäfer and Orlovskii [3-5] on the transport behavior of rare-earth phosphates. The existing analogies regarding the chemical and structural properties [6, 7] of rare-earth phosphates, arsenates and vanadates, as well as the fact that in the literature no information is available about the crystallization of neither rare-earth arsenates nor rare-earth phosphates  $REPO_4$  ( $RE = Dy, Ho, Er, Tm, Yb, Lu$ ) via the gaseous phase, were the motivations to investigate the chemical transport of the arsenates related to the mentioned rare-earth phosphates. The chemical transport is an effective preparative method for the synthesis and crystallization of compounds showing high decomposition pressures at the melting point or, when heated, decomposing before reaching the melting temperature, as is shown by the thermal behavior of rare-earth arsenates [8-13].

This work describes the chemical transport of rare-earth arsenates using different transport agents. Furthermore, it was shown that the rare-earth phosphates of the heavy rare-earth elements can be also crystallized via the gaseous phase. Thus, present investigations on rare-earth arsenates serve as a further example for the chemical transport of rare-earth containing compounds with complex anions.

Quaternary rare-earth transition metal oxide halogenides [14-16] as well as rare-earth niobates, tantalates and titanates [17-20] are substantial examples of chemical transport besides the already mentioned rare-earth phosphates and vanadates.

Starting from 400 mg to 700 mg of a micro-crystalline powder material, the transport experiments (6 to 20 days) were carried out in evacuated quartz glass tubes of 100 mm in length and an inner diameter of 16 mm as an endothermal reaction of  $T_2$  (source) 1333 K to 1353 K to  $T_1$  (sink) 1223 K to 1263 K. The temperature gradients varied between 125 K and 100 K. As transport agents, between 80 mg and 120 mg of  $TeCl_4$ ,  $TeBr_4$ ,  $TeI_4$ ,  $PCl_5$ ,  $PBr_5$ ,  $HgCl_2$  as well as of the mixtures of transport agents of  $S/PtCl_2$ ,  $As/PtCl_2$ ,  $As/Cl_2$ ,  $As/PtBr_2$  and  $As/I_2$  were utilized. The chemical transport by  $TeCl_4$  yielded the rare-earth arsenates  $REAsO_4$  ( $RE = Sc, Y, La - Nd, Sm - Lu$ ) as well as solid solution of rare-earth arsenates. Light-microscopic images of selected examples are shown in Fig. 1 and a list of selected examples of the obtained solid solutions is resumed on Tab. 1. The last mixed rare-earth arsenates were thereby obtained from micro-crystalline powder mixtures of the respective rare-earth arsenates.

Transport experiments on  $NdAsO_4$ , using the other transport agents — apart from  $TeCl_4$  — show that, within the stated range of temperature, all

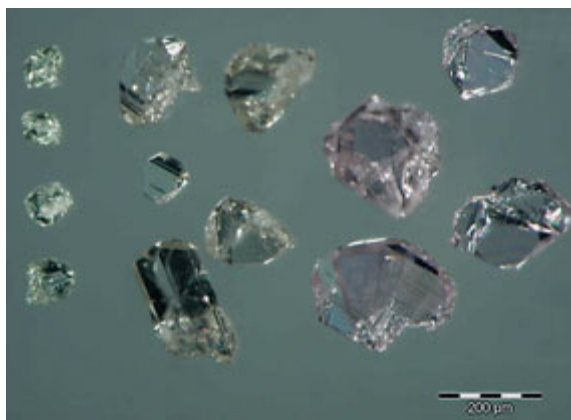


Fig. 1: Light-microscopic image of  $La/PrAsO_4$  (left),  $Pr/NdAsO_4$  (middle) and  $Nd/SmAsO_4$  (right) mixed crystals.

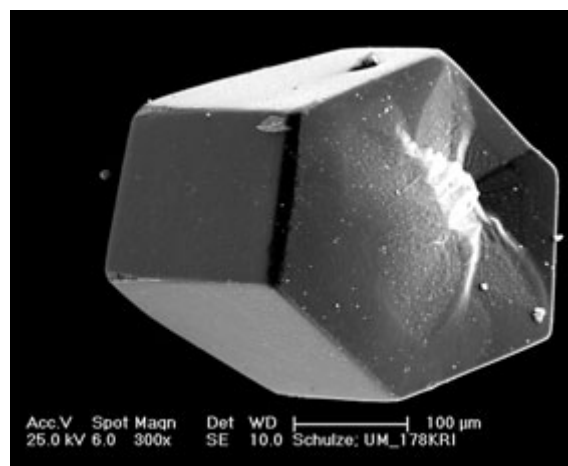


Fig. 2: Secondary electron image of a  $TbAsO_4$  crystal.

chem. composition powder mixture	RE X-ray lines	atomic ratio [at. %]	chem. composition solid solution
La <sub>0.5</sub> Pr <sub>0.5</sub> AsO <sub>4</sub>	La L <sub>α1</sub> , Pr L <sub>β1</sub>	La: 22.34 ± 0.66, Pr: 25.90 ± 0.13, As: 26.79 ± 0.14, O: 24.97	La <sub>0.42</sub> Pr <sub>0.48</sub> AsO <sub>4</sub>
Pr <sub>0.5</sub> Nd <sub>0.5</sub> AsO <sub>4</sub>	Nd L <sub>α1</sub> , Pr L <sub>α1</sub>	Pr: 25.90 ± 0.33, Nd: 24.83 ± 0.27, As: 26.47 ± 0.12, O: 23.27	Pr <sub>0.50</sub> Nd <sub>0.48</sub> AsO <sub>4</sub>
Er <sub>0.5</sub> Yb <sub>0.5</sub> AsO <sub>4</sub>	Er L <sub>α1</sub> , Yb L <sub>α1</sub>	Er: 26.66 ± 0.13, Yb: 28.67 ± 0.19, As: 23.95 ± 0.06, O: 20.73	Er <sub>0.49</sub> Yb <sub>0.51</sub> AsO <sub>4</sub>
La <sub>0.5</sub> Er <sub>0.5</sub> AsO <sub>4</sub>	La L <sub>α1</sub> , Er L <sub>α1</sub>	La: 15.30 ± 0.22, Er: 0.62 ± 0.24, As: 15.84 ± 0.18, O: 68.24	La <sub>0.99</sub> Er <sub>0.04</sub> AsO <sub>4</sub>
		La: 0.67 ± 0.39, Er: 15.77 ± 0.58, As: 16.35 ± 0.27, O: 67.20	La <sub>0.04</sub> Er <sub>0.95</sub> AsO <sub>4</sub>
La <sub>0.25</sub> Er <sub>0.75</sub> AsO <sub>4</sub>	La L <sub>α1</sub> , Er L <sub>α1</sub>	La: 15.53 ± 0.32, Er: 0.71 ± 0.24, As: 16.24 ± 0.14, O: 67.53	La <sub>0.93</sub> Er <sub>0.04</sub> AsO <sub>4</sub>
		La: 0.81 ± 0.40, Er: 15.83 ± 0.46, As: 16.69 ± 0.16, O: 66.68	La <sub>0.04</sub> Er <sub>0.95</sub> AsO <sub>4</sub>
La <sub>0.75</sub> Er <sub>0.25</sub> AsO <sub>4</sub>	La L <sub>α1</sub> , Er L <sub>α1</sub>	La: 14.65 ± 0.42, Er: 0.70 ± 0.55, As: 15.20 ± 0.22, O: 69.45	La <sub>0.87</sub> Er <sub>0.04</sub> AsO <sub>4</sub>
		La: 0.91 ± 0.53, Er: 14.81 ± 0.60, As: 15.45 ± 0.15, O: 68.83	La <sub>0.05</sub> Er <sub>0.89</sub> AsO <sub>4</sub>
La <sub>0.5</sub> Sm <sub>0.5</sub> AsO <sub>4</sub>	La L <sub>α1</sub> , Sm L <sub>α1</sub>	La: 7.97 ± 0.57, Sm: 8.96 ± 0.62, As: 16.47 ± 0.23, O: 66.60	La <sub>0.47</sub> Sm <sub>0.53</sub> AsO <sub>4</sub>
La <sub>0.25</sub> Sm <sub>0.75</sub> AsO <sub>4</sub>	La L <sub>α1</sub> , Sm L <sub>α1</sub>	La: 6.15 ± 0.40, Sm: 9.87 ± 0.39, As: 14.99 ± 0.40, O: 68.99	La <sub>0.38</sub> Sm <sub>0.61</sub> AsO <sub>4</sub>
La <sub>0.75</sub> Sm <sub>0.25</sub> AsO <sub>4</sub>	La L <sub>α1</sub> , Sm L <sub>α1</sub>	La: 13.17 ± 0.36, Sm: 4.21 ± 0.34, As: 17.12 ± 0.2, O: 65.50	La <sub>0.79</sub> Sm <sub>0.25</sub> AsO <sub>4</sub>
Nd <sub>0.5</sub> Sm <sub>0.5</sub> AsO <sub>4</sub>	Nd L <sub>α1</sub> , Sm L <sub>α1</sub>	Nd: 10.42 ± 0.17, Sm: 6.55 ± 0.33, As: 16.62 ± 0.31, O: 66.40	Nd <sub>0.62</sub> Sm <sub>0.38</sub> AsO <sub>4</sub>
Nd <sub>0.5</sub> Eu <sub>0.5</sub> AsO <sub>4</sub>	Nd L <sub>α1</sub> , Eu L <sub>α1</sub>	Nd: 8.27 ± 0.58, Eu: 7.98 ± 0.61, As: 16.88 ± 0.16, O: 66.87	Nd <sub>0.5</sub> Eu <sub>0.48</sub> AsO <sub>4</sub>
Nd <sub>0.5</sub> Gd <sub>0.5</sub> AsO <sub>4</sub>	Nd L <sub>α1</sub> , Gd L <sub>α1</sub>	Nd: 8.96 ± 0.77, Gd: 8.02 ± 1.07, As: 16.84 ± 0.65, O: 66.19	Nd <sub>0.54</sub> Gd <sub>0.38</sub> AsO <sub>4</sub>
Nd <sub>0.5</sub> Er <sub>0.5</sub> AsO <sub>4</sub>	Nd L <sub>α1</sub> , Er L <sub>α1</sub>	Nd: 10.04 ± 1.47, Er: 6.30 ± 1.64, As: 16.31 ± 0.23, O: 67.35	Nd <sub>0.61</sub> Er <sub>0.39</sub> AsO <sub>4</sub>
Nd <sub>0.5</sub> Tm <sub>0.5</sub> AsO <sub>4</sub>	Nd L <sub>α1</sub> , Tm L <sub>α1</sub>	Nd: 10.79 ± 1.31, Tm: 6.31 ± 1.31, As: 16.94 ± 0.33, O: 65.96	Nd <sub>0.64</sub> Tm <sub>0.38</sub> AsO <sub>4</sub>

Tab. 1: Chemical composition of solid solutions of rare-earth arsenates

chlorine and bromine-containing transport agents enable crystallization in endothermal transport for NdAsO<sub>4</sub>, whereas the rates of transport of the bromine-containing systems are smaller, in comparison with the chlorine-containing systems. For iodine containing transport agents, TeI<sub>4</sub> and AsI<sub>2</sub>, no transport of NdAsO<sub>4</sub> was observed under the studied experimental conditions.

The rare-earth phosphates HoPO<sub>4</sub> and ErPO<sub>4</sub> were obtained by chemical transport with PCl<sub>5</sub> as transport agent. Furthermore, all the investigated rare-earth phosphates REPO<sub>4</sub> (RE = Dy, Ho, Er, Tm, Yb, Lu) could be crystallized with endothermal transport using PBr<sub>5</sub> as transport agent.

The reactions of the rare-earth arsenates or phosphates, particularly in the gaseous phase, with the SiO<sub>2</sub> of the tube wall, result in a strong corrosion of the quartz glass tubes. The small transport rates are the reason for the transport times of more than 2 weeks to get an acceptable amount (100 to 400 mg) of transported crystals. Typical transport rates of 1 mg/h were observed for the described systems.

Selected crystals were analysed by means of scanning electron microscopy (SEM, Philips XL30) and electron micro-probe analyzer (Cameca SX 100). For the accurate determination of the chemical composition by energy-dispersive and wavelength-dispersive X-ray spectroscopy (EDXS and WDXS, respectively) representative well-faceted crystals with dimensions of nearly 100 µm were embedded in resin (Technovit 200LC, Spezifix20+TEKMEK, or Polyfast) with appropriate hardness and viscosity for metallographic analysis. The polished surfaces were covered with thin carbon layers by sputter technique due to the insulting properties of the investigated phases. The majority phase showed homogenous material contrast in the back scatter electron mode. Quantitative analyses were performed on a microprobe by WDXS method with 25 keV / 40 nA electron beam. In general, counting time of 30 sec was used to determine the intensities of RE L<sub>α</sub> and As K<sub>α</sub> X-ray lines which were selected by PET or LiF monochromator crystals. The energy resolution of the X-

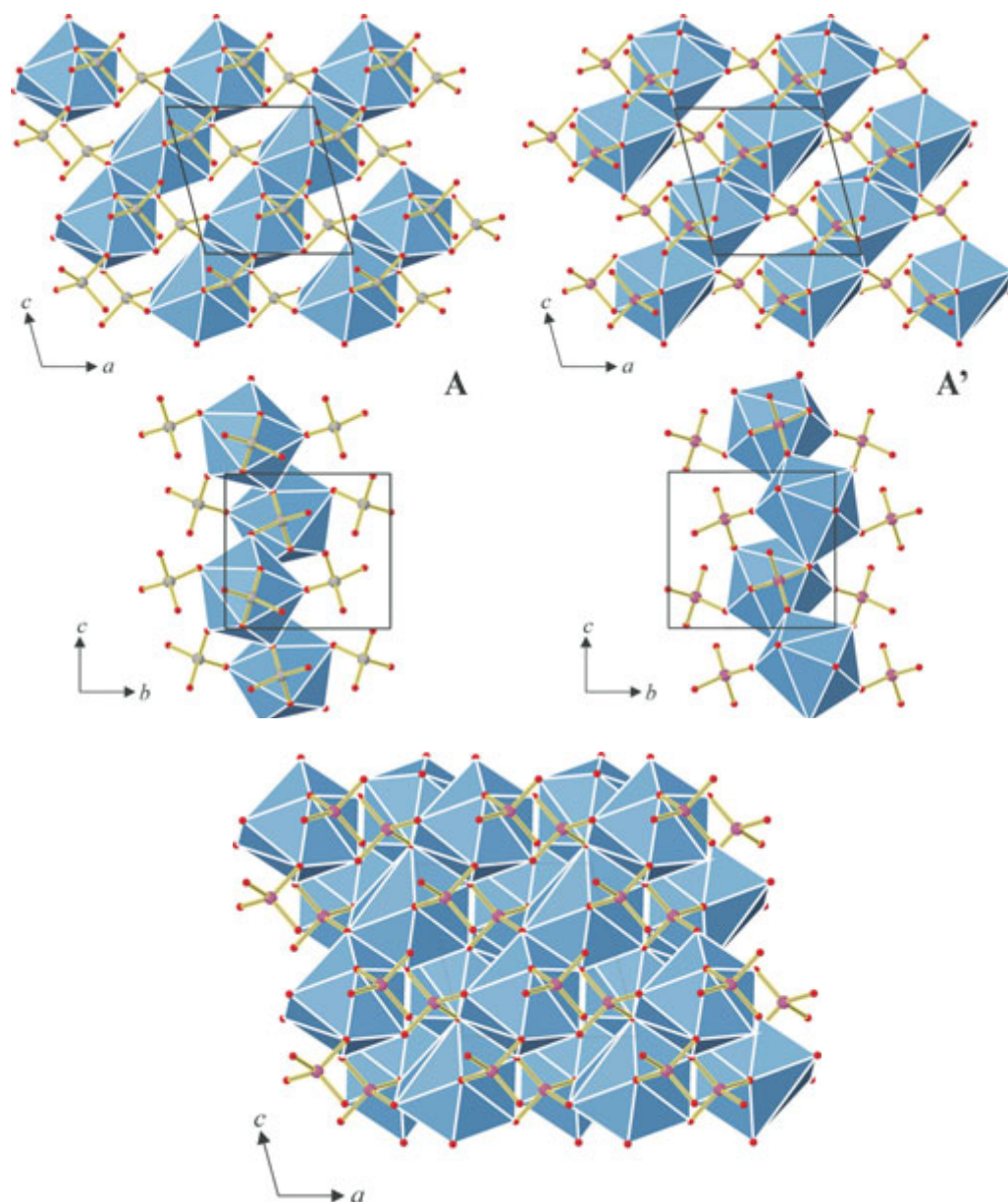


Fig. 3: a) Projection of the crystal structure of the rare-earth arsenates of the monoclinic monazite type along  $[010]$  (below) as a resulting combination of the two A and A' layers, shown above. b) Combination of A and A' layers.

ray detection allows to use RE  $L\alpha$  lines also for quaternary compounds with two rare-earth elements. The much weaker Pr  $L\beta$  line has to be used due to strong overlap of Pr  $L\alpha$  and La  $L\beta$  for  $\text{La}_{1-x}\text{Pr}_x\text{AsO}_4$ . Special care was applied to select appropriate reference materials to get reliable data for chemical composition of the new ternary and quaternary compounds. The RE fluorides were used to calibrate the RE content as far as they are available; the intensities of As  $K\alpha$  lines were calibrated in respect of elemental As. Ternary arsenates with

related RE content (e.g.  $\text{LaAsO}_4$ ) were used as references for compounds with two rare earth elements. The oxygen content was calculated from individual contributions of the other two or three elements of the compound and was defined as the mass concentration residue. In all cases, the atomic ratio of As and O was acceptable close to 1:4 and the overall RE and arsenic contents are quite similar. Compositions of the quaternary phases are collected in Tab. 1. The average values of ten measurements are given.

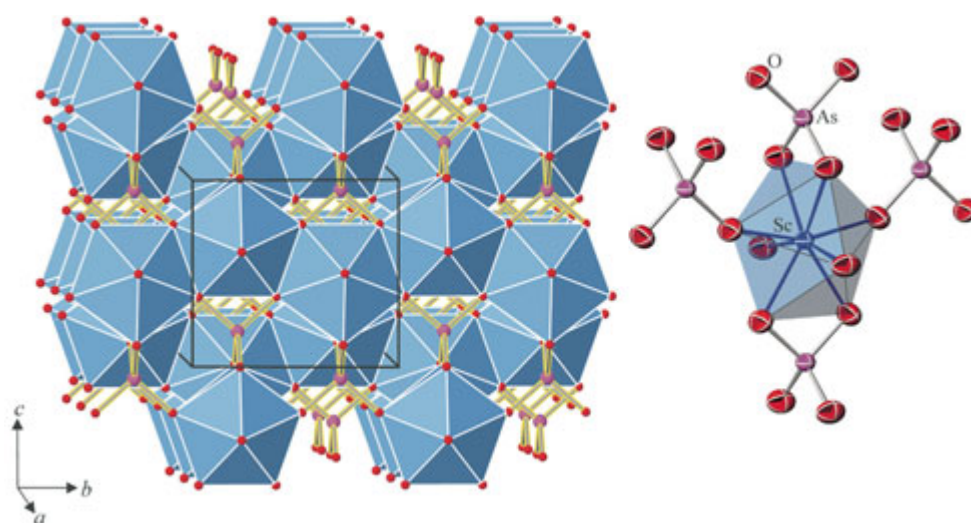


Fig. 4: Projection of the crystal structure along  $[100]$  of the rare-earth arsenates crystallizing in the tetragonal xenotime type (left) and the respective coordination polyhedron of the rare-earth ion (right).

Rare-earth phosphates and arsenates crystallize in different structure types depending on the ionic radius of the rare-earth cation and the central atom of the complex anion as well as on pressure and temperature. From previous X-ray diffraction investigations on powders [6] and on single crystals structure analysis for  $\text{CeAsO}_4$  [21],  $\text{TbAsO}_4$  and  $\text{DyAsO}_4$  [22] as well as  $\text{LuAsO}_4$  [23], it is known that, under ambient conditions, the rare-earth arsenate of large rare-earth ions crystallize in the monazite type (monoclinic, space group  $P2_1/n$ ), while those of small rare-earth ions occur in the xenotime type (tetragonal,  $I4_1/amd$ ). In this work, refinements of the crystal structures of  $\text{LaAsO}_4$  and  $\text{NdAsO}_4$  as well as of  $\text{SmAsO}_4$ ,  $\text{HoAsO}_4$  and  $\text{ScAsO}_4$  were performed from X-ray single crystal diffraction data of the species synthesized by chemical transport with  $\text{TeCl}_4$ . The lattice parameters were determined on the basis of powder data by least squares refinement with the program package WinCSD [24].

### The Monazite Type

The refinement of the crystal structure of lanthanum and neodymium arsenate was carried out in the space group  $P2_1/n$  (no. 14). Arsenic is tetrahedrally coordinated by four oxygen atoms, while the rare-earth cation is surrounded by nine oxygen atoms. A possible description of the crystal structure can be made considering the  $[\text{REO}_9]$  polyhedron. Two lay-

ers  $A$  and  $A'$  can be recognized in the framework (Fig. 3a), which form an alternating  $AA'AA'$  sequence along  $[010]$ , whereas  $A'$  occurs by turning and shifting ( $2_1$ ) of the  $A$  layer. Within the layer,  $[\text{REO}_9]$  polyhedra condense chain-like sharing common edges parallel to  $[011]$ . At the same time, they are linked with  $[\text{AsO}_4]$  tetrahedra via common edges. Between  $A$  and  $A'$  layers, the  $[\text{REO}_9]$  polyhedra are connected to the  $[\text{AsO}_4]$  tetrahedra by common edges as well as by common corners.

Considering an isolated  $[\text{REO}_9]$  polyhedron, seven of the oxygen atoms are allocated to respectively different  $[\text{AsO}_4]$  tetrahedra, whereas five of them are linked with the polyhedron by common corners and two of them by common edges. These two edge-linked tetrahedra are aligned parallel to the  $a$ -axis and twisted against each other by  $90^\circ$ .

### The Xenotime Type

Scandium, samarium and holmium arsenates crystallize tetragonally in the space group  $I4_1/amd$  (no. 141). The rare-earth ion is surrounded by eight oxygen atoms, whereas six of them belong to four different  $[\text{AsO}_4]$  tetrahedra (Fig. 4b). Analog to the description of the rare-earth arsenates of the monazite type, the  $[\text{REO}_8]$  polyhedron (bisdisphenoid) can be considered as principal building unit of the structure. They are condensed by common edges and form interpenetrating chains parallel to  $[100]$  and  $[010]$ . This creates a three-dimensional frame-

work, which is interconnected via edge-linked tetrahedra in the direction of  $c$  (Fig. 4a).

Two of the coordinating  $[\text{AsO}_4]$  tetrahedra are connected to an isolated  $[\text{REO}_8]$  polyhedron in equatorial position through common corners and two in axial position of the bisdisphenoid through common edges (Fig. 4b). These opposite edges are twisted  $90^\circ$  one to each other and inside the network, they are aligned parallel to  $[001]$ . The distortion of the  $[\text{AsO}_4]$  tetrahedron can be recognized in both the holmium and the scandium arsenate considering the interatomic distances and angles.

For the thermodynamic description as well as for model calculations, simulations and thus for prediction of the optimal transport conditions, it is necessary to know all condensed and all gaseous species present in the system and their thermodynamic data. First thermodynamical model calculations for describing the solid-phase/gaseous-phase equilibria, the composition of the gaseous phase as well as the temperature dependent partial pressure courses and transport efficiency of the various species were carried out with the program package TRAGMIN [25]. The calculations are based on minimizing the free enthalpy of the system in accordance with Eriksson's method [26].

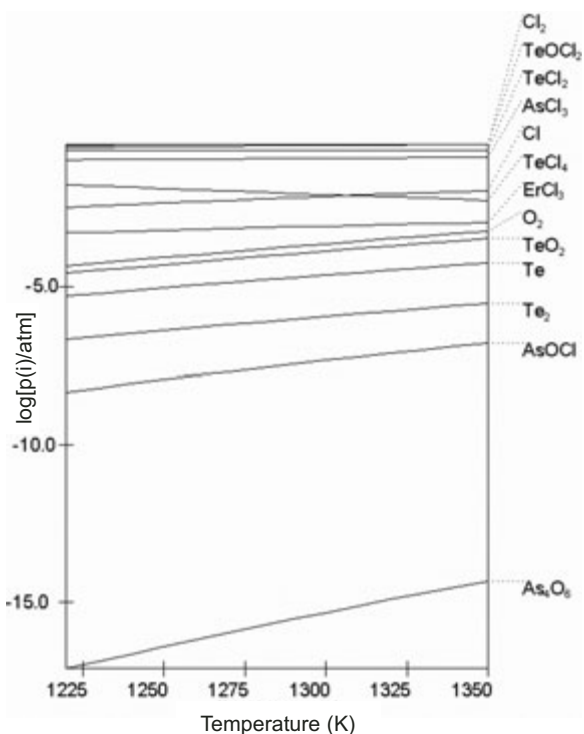


Fig. 5: Calculated gaseous phase composition above  $\text{ErAsO}_4$ , being in equilibrium with  $\text{TeCl}_4$ , for the temperature range from 1225 K to 1350 K.

As representative for the rare-earth arsenates investigated, the calculated gaseous phase composition above an  $\text{ErAsO}_4$  source, which is in equilibrium with  $\text{TeCl}_4$  is shown, in the temperature range from 1225 K to 1350 K (Fig. 5). The dominating gaseous species are  $\text{Cl}_2$  and  $\text{TeCl}_2$ , which are formed by thermal decomposition from the transport agent  $\text{TeCl}_4$ , and  $\text{TeOCl}_2$  as previously described by Oppermann [27]. Usually, the formation of  $\text{TeOCl}_2$  [28] in oxidic systems allows a decrease in the partial pressure of oxygen, in the present case in a range of  $10^{-4}$  bar. This suppresses the formation of rare-earth oxide halogenides and thus the transport of rare-earth oxo compounds is allowed. Furthermore, it can be shown that principally  $\text{AsCl}_3$  should be the arsenic-transporting species. The partial pressures of the other arsenic species  $\text{AsOCl}$  and  $\text{As}_4\text{O}_6$  clearly range below  $10^{-5}$  bar, thus do not have any transport effect. The rare-earth component is exclusively transported via the respective rare-earth trichloride, in the present case being  $\text{ErCl}_3$ . With the help of the calculated efficiency of transport (Fig. 6), it is possible to describe the observed endothermal transport behavior of  $\text{ErAsO}_4$ , representatively for the rare-earth arsenates in good approximation by the fol-

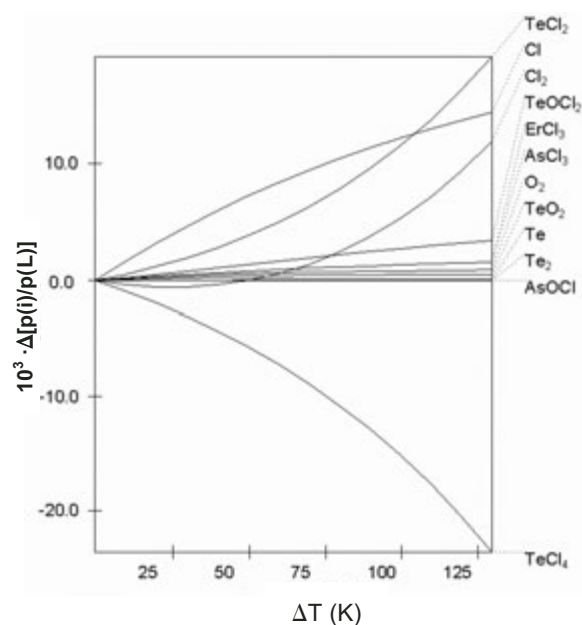
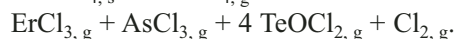
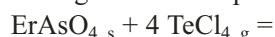


Fig. 6: Calculated transport efficiency of the gaseous phase species for the chemical transport of  $\text{ErAsO}_4$  by  $\text{TeCl}_4$  (of 1350 K after 1225 K for 3 g of micro-crystalline powder material and 100 mg  $\text{TeCl}_4$  with a cross-section of  $2 \text{ cm}^2$  and a diffusion distance of 100 mm).

lowing formal transport equilibrium:



First quantitative transport calculations representing a simulation of the experiment, result in relatively good agreement between the calculated (0.7 mg/h)

and experimental (approx. 0.2 mg/h) transport rate, so that it can be assumed that the chemical transport of rare-earth arsenates is described correctly with the applied model. This model is based on condensed phases and gaseous phase species involved with their thermodynamic data.

## References

- [1] *K. Matsumoto, T. Kawanishi and K. Takagi*, J. Cryst. Growth, **55** (1981) 376.
- [2] *M. Schmidt, R. Ramlau, W. Schnelle, H. Borrmann, E. Milke and M. Binnewies*, Z. Anorg. Allg. Chem. **631** (2005) 284.
- [3] *H. Schäfer and V. P. Orlovskii*, Z. Anorg. Allg. Chem. **390** (1972) 13.
- [4] *V. P. Orlovskii, H. Schäfer, V. P. Repko, M. Safronov and I. V. Tananaev*, Neorg. Mater. **7** (6)(1971) 971.
- [5] *V. P. Repko, V. P. Orlovskii, M. Safronov, Kh. Kurbanov, M. N. Tseitlin, V. I. Pakhomov, I. V. Tananaev and A. N. Volodina*, Neorg. Mater. **7** (2) (1971) 251.
- [6] *H. Schwarz*, Z. Anorg. Allg. Chem. **323** (1963) 44.
- [7] *U. Kolitsch and D. Holtstam*, Eur. J. Mineral. **16** (2004) 117.
- [8] *H. Schäfer*, Chemische Transportreaktionen, Verlag Chemie, Weinheim (1962).
- [9] *R. Gruehn and R. Glaum*, Angew. Chem. In. Ed. **39** (2000) 692.
- [10] *F. Emmenegger*, J. Crystal Growth, **3/4** (1968) 135.
- [11] *H. Schäfer*, J. Crystal Growth, **9** (1971) 17.
- [12] *E. Kaldis*, Principles of the Vapour Growth of Single Crystals, in Crystal Growth, Theory and Techniques, C. H. L. Goodman, Plenum Press (1974).
- [13] *K.-Th. Wilke and J. Bohm*, Kristallzüchtung, Verlag Harri Deutsch, Thun, Frankfurt/Main (1988).
- [14] *N. Hübner, U. Schaffrath and R. Gruehn*, Z. Anorg. Allg. Chem. **591** (1990) 107.
- [15] *N. Hübner and R. Gruehn*, Z. Anorg. Allg. Chem. **602** (1991) 119.
- [16] *M. Thomas and R. Gruehn*, J. Solid State Chem. **99** (1992) 219.
- [17] *R. Hoffmann*, Dissertation, Universität Gießen (1993).
- [18] *U. Schaffrath*, Dissertation, Universität Gießen (1989).
- [19] *J. Sturm*, Dissertation, Universität Gießen (1976).
- [20] *R. Ross and R. Gruehn*, Z. Anorg. Allg. Chem. **591** (1990) 95.
- [21] *A. Brahim, F. Mohamed Mongi and H. Amor*, Acta Cryst. **58** (2002) 98.
- [22] *F. G. Long and C. V. Stager*, Can. J. Phys. **55** (1977) 1633.
- [23] *G. Lohmüller, G. Schmidt, B. Deppisch, V. Gramlich and C. Scheringer*, Acta Cryst. **B29** (1973) 141.
- [24] *L. G. Aksehrud, P. Yu. Zavalli, Yu. Grin, V. K. Pecharsky, B. Baumgartner, E. Wölfel*, Mater. Sci. Forum, **335** (1993) 133.
- [25] *G. Krabbes, W. Bieger, K.-H. Sommer, T. Söhnel*, Programmpaket TRAGMIN, IFW Dresden, TU Dresden, Institut für Anorganische Chemie (1995).
- [26] *G. Eriksson*, Acta Chem. Scand. **25** (1971) 2651.
- [27] *H. Oppermann*, Z. Anorg. Allg. Chem. **434** (1977) 239.
- [28] *H. Oppermann and M. Ritschel*, Krist. Tech. **10** (1975) 485.